Acta Oceanol. Sin., 2019, Vol. 38, No. 9, P. 102–112
https://doi.org/10.1007/s13131-019-1478-9
http://www.hyxb.org.cn
E-mail: hyxbe@263.net

A numerical model with Stokes drift for pollutant transport within the surf zone on a plane beach

Chunping Ren[1, 2*], Rongrong Liang[1], Chong Yu[1], Yuchuan Bai[2]

[1] College of Water Resource Science and Engineering, Taiyuan University of Technology, Taiyuan 030024, China

[2] State Key Laboratory of Hydraulic Engineering Simulation and Safety, Tianjin University, Tianjin 300072, China

Received 1 May 2018; accepted 3 September 2018

Abstract

This study examines the effects of Stokes drift on pollutant transport within the surf zone on a plane beach both numerically and experimentally. Firstly, the numerical model is described. The wave-induced current is modeled using the concept of the radiation stress. The wave propagation model is based on the wave energy conservation equation. And the advective diffusion model including the Stokes drift is used to describe the pollutant transport in the surf zone. Model validation was achieved in this case versus an analytical solution for an instantaneous point source in a uniform horizontal flow. This study also describes a laboratory experiment on dye release in the surf zone over a plane beach. We examined the final inclination angle required by a continuously released pollutant plume to reach the shoreline under both cases, and transport velocities in the alongshore and cross-shore directions were estimated by linearly fitting the location of a dye-patch front at different time. Results show that this dye patch moved shoreward with an approximate speed of 0.05 m/s (0.017 m/s) between 10 s and 40 s and 0.001 m/s (0.011 m/s) after 40 s for Case 1 (2). This model was then used to simulate pollutant transport in the surf zone on a plane beach as reproduced in the current experiment. Comparisons between our dye transport experiment and numerical results were then also conducted; the data showed that the numerical results including Stokes drift agreed more closely with experimental results than those without it. The data showed that the pollutant was generally transported obviously shoreward in addition to its expected drift along the shore. We also suggest that Stokes drift plays an important role in pollutant movement in the surf zone, especially shoreward.

Key words: nearshore current model, Stokes drift, advection diffusion, dye release, surf zone

Citation: Ren Chunping, Liang Rongrong, Yu Chong, Bai Yuchuan. 2019. A numerical model with Stokes drift for pollutant transport within the surf zone on a plane beach. Acta Oceanologica Sinica, 38(9): 102–112, doi: 10.1007/s13131-019-1478-9

1 Introduction

The frequency of pollutant loading through both the shoreline and the seaward boundary increases in the nearshore zone due to increases in recreational and commercial activities. Increasing heavy pollutant inputs into the nearshore zone threaten economic and environmental resources (Hally-Rosendahl et al., 2014). It is therefore critically important to understand pollutant transport to manage conflicts efficiently between waste drainage, recreation and fisheries.

Stokes drift is a phenomenon that occurs in the uppermost ocean layer in response to wind, waves and currents and is important in transporting plastics, oil and pollution within different layers of the water column both in surf and in deep-water zones (Curcic et al., 2016; Iwasaki et al., 2017; Weisberg et al., 2017; Myrhaug et al., 2018). Stokes drift exerts a considerable influence on pollution transport within the surf zone because of mass flux inertia, even to some extent if waves break within this area. Current knowledge of the quantitative impact of Stokes drift within the surf zone remains poor, however, because of the complex processes involved. The purpose of this paper is therefore to investigate the effects of Stokes drift on pollutant transport in the surf zone using advection and diffusion equations that address this process in combination with experimental results.

Extensive field measurements have been carried out on dye transport and mixing within the surf zone. Numerous researchers have used fluorescent dye tracers to investigate surf-zone diffusivity at the shoreline (Harris et al., 1963; Inman et al., 1971; Grant et al., 2005; Clarke et al., 2007). Researchers have estimated diffusivity by measuring the horizontal spreading rate of a fluorescent dye tracer. In one study, Clark et al. (2010) estimated the cross-shore surf-zone dispersion of a continuously released dye tracer in an alongshore current by measuring tracer concentrations. It has also been suggested that surf-zone eddies induced by either shear instabilities or finite-crest-length wave breaking also plays an important role in tracer dispersion. All these visual field observations show that tracer patches released into the surf zone at beaches that are alongshore-uniform generally remain within a few surf-zone widths of the shoreline over the next few hours (Clark et al., 2010). Previous workers have not, however, analyzed the role played by Stokes drift in tracer transport. It is clear that this process is one manifestation of ocean surface waves and that it influences mass and momentum transport adjacent to the surface. The motivation for this study was therefore a desire to achieve a better understanding of the effects

Foundation item: The Open Foundation of the State Key Laboratory of Hydraulic Engineering Simulation and Safety under contract No. HESS-1406; the National Science Foundation for Post-doctoral Scientists of China under contract No. 2013M541179; the Foundation of Taiyuan University of Technology under contract No. 2017MS07.

*Corresponding author, E-mail: chunpingren@163.com

of Stokes drift on pollutant transport in the nearshore zone. In one previous study, Hally-Rosendahl et al. (2014) suggested that transient rip current ejection events play a significant role in pollutant exchange between the surf zone and the inner shelf and estimated that Stokes drift-driven cross-shore exchange is therefore small in places where rip currents are present. This result built on earlier work in which Lentz et al. (2008) had suggested that Stokes drift-driven exchange may be important to a seaward distance of $2x_b$ (where x_b denotes the seaward surf-zone boundary). Stokes drift may also play an important role in pollutant transport if waves are obliquely incident or in cases where rip currents are weak. It is therefore also meaningful to investigate the effects of this process on pollutant transport in an alongshore current. However, the lack of high-quality synchronized experimental data makes transport modeling, including the validation of Stokes drift, problematic. We are therefore particularly interested in evaluating the influences of this process through comparisons between high-quality experimental images of the surf zone and numerical models.

Pollutant transport in the surf zone has been modeled both analytically and numerically (Harris et al., 1963; Inman et al., 1971; Clarke et al., 2007). In one study, Xu and Chua (2016) developed the nested three-dimensional (3-D) unstructured-grid model to simulate flow and pollutant transport in coastal waters around Singapore. These workers demonstrated that transport, coupled circulation, and wave models are needed to predict pollutant transport; they focused, however, on surf-zone diffusivity value parameterizations in their models, even though these variables have not been validated over a broad range of conditions (Clark et al., 2011) and the relationship between the diffusivity coefficients and the trajectory of maximum concentration within this zone has not been addressed in any detail (Brown et al., 2009; Pearson et al., 2009; Clark et al., 2011). Furthermore, numerical studies such as this have not placed much emphasis on the role that Stokes drift does play in pollution transport in nearshore zone; this is important because accurately predicting the trajectory of this movement is very important for designing marine outfalls. The trajectory of Stokes drift might exert a significant influence on sewage discharge facility site selection. In this context, Winckler et al. (2013) defined the distance between the source and the landing position as the contact distance. It is clear that both hydrodynamic conditions and Stokes drift can considerably influence transport direction; of these, the former have been well described in wave and circulation models. At the same time, however, Stokes drift (mass transport) has not attracted a great deal of attention in either field experimental investigations or numerical simulation of pollutant transport in the nearshore zone. In one study, Winckler et al. (2013) developed an advective diffusion equation that describes transport within the surf zone. The advective terms in this equation include the contribution of Stokes drift, a component that has been largely ignored in many existing surf-zone pollutant transport models.

The wave field on a plane beach with a constant slope is modeled in this study using linear theory, whereas the flow field is predicted on the basis of Longuet-Higgins theory (Longuet-Higgins, 1970a, b). Our approach is distinct because diffusivities, including interaction between waves and currents, are used in the transport equation, unlike the diffusivity equations used by Winckler et al. (2013). The wave and circulation model as well as the solute transport equation are solved in our approach using an alternating direct-implicit (ADI) finite-difference scheme. All models were run until a steady state was achieved.

The paper is structured as follows: Section 2 gives a model description, including the three sub-models: (1) the wave model; (2) the nearshore wave-induced current model; and (3) the pollutant transport model. Section 3 briefly describes the experimental setup. Section 4 summarizes the results of detailed model comparison with these data sets. Finally, conclusions are given in Section 5.

2 Numerical models

Various kinds of wave theories and transformation models are available for monochromatic, random, linear and nonlinear waves passing over a uniform sea bottom or arbitrary bathymetry (Tang et al., 2016, 2017). A wave transformation model based on the wave energy equation was used here due to the particular bed form. The energy dissipation term was formulated in this study following Battjes and Janssen (1978) and Roelvink (1993).

An alongshore current is generated when waves propagate obliquely to the shoreline and break; thus, a nearshore current field is determined based on the depth-averaged model. Longuet-Higgins (1970a, b) established the concept of radiation stress, the excess momentum flux due to the presence of waves. Wave-induced circulation forcing is usually parameterized with radiation stress.

2.1 *Wave transformation model*

Wave transformation is modeled using the wave energy balance equation as follows:

$$\frac{\partial E_w c_g \cos\theta}{\partial x} = -S, \tag{1}$$

where E_w denotes wave energy, c_g is the group velocity, θ is the angle of incidence with respect to the shore normal, and S is the dissipation term. Wave incidence angle was obtained from Snell's law, and group velocity was calculated as follows:

$$c_g = \left(\frac{1}{2} + \frac{kh}{\sinh(2kh)}\right) c, \tag{2}$$

where c is the phase speed and k is the wave number.

Wave energy, E_w, can be expressed as follows:

$$E_w = \frac{\rho g H^2}{8}. \tag{3}$$

The dissipation of regular and irregular waves was modeled following Battjes and Janssen (1978) and Roelvink (1993) as follows:

$$S = \begin{cases} \dfrac{\rho g}{4T_p}\alpha H^2 Q_b & \text{regular waves,} \\ \left\{1 - \exp\left[-\left(\dfrac{H_{rms}}{\gamma h}\right)^n\right]\right\} 2\alpha f_p E_w & \text{random waves,} \end{cases} \tag{4}$$

where T_p is the peak period, H is the wave height, Q_b is the probability of wave breaking, H_{rms} is the root mean square wave height, γ is the wave breaking parameter, f_p is the peak frequency, and n and α are empirical coefficients such that $n = 10$ and α=0.25 (Roelvink, 1993). Wave heights in the computational domain were obtained using Eqs (1) to (4), and radiation stresses were obtained using wave heights and directions as follows:

$$S_{xx} = S_{11}\cos^2\theta + S_{22}\sin^2\theta, \tag{5}$$

$$S_{yy} = S_{11}\sin^2\theta + S_{22}\cos^2\theta, \tag{6}$$

$$S_{xy} = S_{yx} = S_{11}\cos\theta\sin\theta - S_{22}\sin\theta\cos\theta, \tag{7}$$

$$S_{ij} = E\begin{pmatrix} \frac{1}{2} + \frac{2kh}{\sinh 2kh} & 0 \\ 0 & \frac{2kh}{\sinh 2kh} \end{pmatrix} (i,\ j = 1,2)\,. \tag{8}$$

The wave breaking point was obtained from the wave model proposed by Baldock et al. (1998) as follows:

$$H_b = \gamma h, \tag{9}$$

where γ is the breaker parameter. In their earlier work, Apotsos et al. (2008) suggested that this parameter can be chosen within the γ=0.73−1.03 range, depending on type.

2.2 *Nearshore current model*

The depth-integrated equations of mass and momentum conservation can be written as follows:

$$\frac{\partial d}{\partial t} + \frac{\partial (Ud)}{\partial x} + \frac{\partial (Vd)}{\partial y} = 0, \tag{10}$$

$$\frac{\partial U}{\partial t} + U\frac{\partial U}{\partial x} + V\frac{\partial U}{\partial y} + g\frac{\partial \bar{\eta}}{\partial x} + \frac{1}{\rho d}\left(\frac{\partial S_{xx}}{\partial x} + \frac{\partial S_{xy}}{\partial y}\right) + \frac{1}{\rho d}\tau_{bx} - A_{mx} = 0, \tag{11}$$

$$\frac{\partial V}{\partial t} + U\frac{\partial V}{\partial x} + V\frac{\partial V}{\partial y} + g\frac{\partial \bar{\eta}}{\partial y} + \frac{1}{\rho d}\left(\frac{\partial S_{yx}}{\partial x} + \frac{\partial S_{yy}}{\partial y}\right) + \frac{1}{\rho d}\tau_{by} - A_{my} = 0, \tag{12}$$

where x and y denote the horizontal coordinates normal and parallel to the shoreline respectively, t is time, U and V are horizontal velocities in the cross-shore and alongshore direction respectively, $\bar{\eta}$ is mean surface elevation, ρ is seawater density, g is gravitational acceleration, h is still water depth, $d = h + \bar{\eta}$, (S_{xx}, S_{xy}, S_{yx}, S_{yy}) are the radiation stresses, τ_{bx} and τ_{by} are bottom stresses in the x- and y-directions respectively, and A_{mx} and A_{my} are turbulent stresses.

The parameters τ_{bx} and τ_{by} in Eqs (11) and (12) were modeled using the linear damping terms proposed by Özkan-Haller and Kirby (1999) and Zhao et al. (2003) as follows:

$$\tau_{bx} = \frac{4}{\pi}\rho c_f u_0 U, \tag{13}$$

$$\tau_{by} = \frac{2}{\pi}\rho c_f u_0 V, \tag{14}$$

where c_f is the bottom friction coefficient and u_0 is the amplitude of the horizontal orbital velocity of incident waves.

The parameters A_{mx} and A_{my} therefore denote the effects of lateral mixing due to turbulence and depth variation in current velocities respectively (Svendsen and Putrevu, 1994). Depth-integrated lateral mixing can therefore be expressed using an eddy viscosity model as follows:

$$A_{mx} = \frac{\partial}{\partial x}\left(\mu\frac{\partial U}{\partial x}\right) + \frac{\partial}{\partial y}\left(\mu\frac{\partial U}{\partial y}\right), \tag{15}$$

$$A_{my} = \frac{\partial}{\partial x}\left(\mu\frac{\partial V}{\partial x}\right) + \frac{\partial}{\partial y}\left(\mu\frac{\partial V}{\partial y}\right), \tag{16}$$

where $\mu = N' x_b\sqrt{gh}$ is the lateral mixing coefficient, $N' = 0$–0.016 denotes the nondimensional coefficient, and x_b is the distance from the wave breaking point to the shoreline.

2.3 *Pollutant advection diffusion model*

In their earlier study, Winckler et al. (2013) derived a transport equation using a multiple-scale perturbation method based on the fact that the time scale of horizontal diffusion is much longer than the wave period. The two advective terms in the transport equation that they developed therefore encompass contributions from the covariance of fluctuating velocity and concentration, which are equivalent to Stokes drift in periodic waves (Tamura et al., 2012).

The transport equation developed by Winckler et al. (2013) can be written as follows:

$$\frac{\partial C}{\partial t} + \left[U - \alpha_s\frac{(gkA)^2}{2\omega^3}\right]\frac{\partial C}{\partial x} + \left[V + \beta_s\frac{(gkA)^2}{2\omega^3}\right]\frac{\partial C}{\partial y} = \frac{1}{d}\frac{\partial}{\partial x}\left(dK_x\frac{\partial C}{\partial x}\right) + K_y\frac{\partial^2 C}{\partial y^2} + S_m, \tag{17}$$

where C denotes depth-averaged concentration, K_x and K_y are the cross-shore and alongshore turbulent diffusivities respectively, and S_m is the source term. Similarly, $\alpha_s = k\cos\theta$, $\beta_s = k\sin\theta$, θ is the angle of incidence with respect to the normal shore, k is the wave number, and A and ω denote wave amplitude and incident wave frequency respectively.

The depth-averaged diffusion coefficients (K_x and K_y) were then calculated as follows:

$$K_x = K_{cx} + K_{wx}, \tag{18}$$

$$K_y = K_{cy} + K_{wy}, \tag{19}$$

$$K_{cx} = \frac{\left(k_l U^2 + k_t V^2\right)h\sqrt{g}}{C_z\sqrt{U^2+V^2}}, \tag{20}$$

$$K_{cy} = \frac{\left(k_l V^2 + k_t U^2\right)h\sqrt{g}}{C_z\sqrt{U^2+V^2}}, \tag{21}$$

$$K_{wx} = K_{wy} = 0.035\alpha_1\frac{h\bar{\eta}}{T}, \tag{22}$$

where K_{cx} and K_{cy} are diffusion coefficients in the cross-shore and alongshore directions under pure currents, K_{wx} and K_{wy} denote turbulent diffusivities under pure waves, and k_l and k_t are depth-averaged longitudinal dispersion and lateral turbulent diffusion coefficients, set to 5.93 and 0.23 respectively. T is the incid-

ent wave period, C_z is the Chezy coefficient, n_s is the Manning coefficient, $C_z = d^{1/6}/n_s$, and α_1 is the empirical parameter modified after van Rijn (1986) and Sun and Tao (2006) in this study. This parameter was calculated as follows:

$$\alpha_1 = \begin{cases} 5.5H/h - 2.0 & \text{breaking zone,} \\ 1.0 & \text{non} - \text{breaking zone.} \end{cases} \quad (23)$$

As discussed by Winckler et al. (2013), advective velocity consists of two parts when modeled using the transport Eq. (17). Hence, components U and V denote the near-shore circulation induced by breaking waves calculated using Eqs (10) to (12), whereas $\alpha (gkA)^2/(2\omega^3)$ and $\beta (gkA)^2/(2\omega^3)$, which are identical to Stokes drift for monochromatic waves, arise from cross correlations between flow fluctuations and concentration. These relationships mean that Stokes drift depends on incident waves, and therefore the Eulerian mean current as well as this process drive dye transport. Two well-known classical approaches, Eulerian and Lagrangian, can be used to obtain the magnitude of the mass flux. Although the vertical distribution of drift velocities differs between the two approaches, vertically integrated volume flux is identical in the case of no vegetation (Jacobsen, 2016). Stokes drift in this analysis was therefore depth-averaged, and the available depth-integrated equations for mass and momentum conservation were used only to simulate the nearshore circulation current.

The boundary condition for the solute was calculated as follows:

$$\partial C/\partial n = 0. \quad (24)$$

This expression means that total concentration changes parallel to the closed boundary and there will be no solute flux across this line. n refers to the direction perpendicular to the closed boundary.

An alternating direct implicit (ADI) function was then used to solve Eqs (10), (11), (12) and (17). In this approach, a single time step is divided into two half-steps such that an explicit scheme is first applied in the x-direction to the implicit scheme in the y-direction, followed by the implicit scheme in the derivatives related to x at the second half time step, and then in derivatives related to y. A tri-diagonal $\bar{\eta}$ matrix is then obtained that can be readily solved for each half time step; a regular staggered uniform grid system was used (Fig. 1). The velocity values U and V are defined on this staggered grid at the positions marked "circle" and "square" (Fig. 1), whereas the wave surface elevation and concentration were stored at the "cross" position. The Courant stability criterion was then used to guide the choice of time step as outlined by Ebersole and Dalrymple (1980) as follows:

$$\Delta t \leqslant \frac{\sqrt{(\Delta x)^2 + (\Delta y)^2}}{\sqrt{g h_{\max}}}, \quad (25)$$

where Δx and Δy are spatial discretizations in the x- and y-directions respectively.

2.4 *Model validation*

To validate the model used in this study, numerical results were compared with analytical solutions from Eq. (26). The solution for an instantaneous point source in a uniform horizontal flow was therefore computed using Eq. (26).

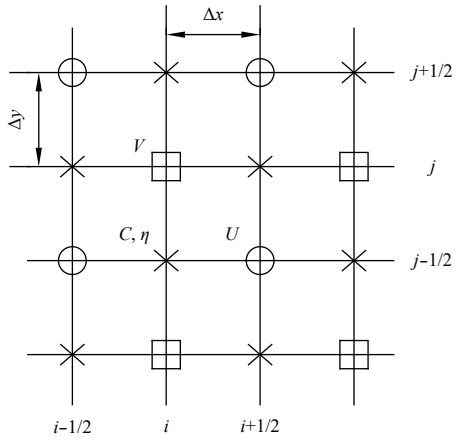

Fig. 1. Sketch map of staggered grid.

The analytical expression for the transport of a Gaussian pulse of unit height can be written as follows:

$$C(x,y,t) = \frac{1}{4t+1} \times \exp\left[-\frac{(x-1.0-U_e t)^2}{K_x(4t+1)} - \frac{(y-1.0-V_e t)^2}{K_y(4t+1)}\right]. \quad (26)$$

The domain for this test was defined as $0 \leqslant x \leqslant 4$ m and $0 \leqslant y \leqslant 4$ m. Hence, the Gaussian pulse of unit height was initially located at (1.0 m and 1.0 m) such that the initial condition could be expressed as follows:

$$C(x,y,0) = \exp\left[-(x-1.0)^2/K_x - (y-1.0)^2/K_y\right]. \quad (27)$$

The parameters in Eq. (26) were chosen to include the uniform horizontal velocities $U_e = V_e = 0.8$ m/s, a grid spacing $\Delta x = \Delta y = 0.025$ m, a time step $\Delta t = 0.001\ 25$ s, and the diffusion coefficients in the x- and y-directions expressed by $k_x = k_y = 0.1$ m^2/s. Figure 2 shows a 3-D perspective view of the initial Gaussian pulse, and Fig. 3 compares the concentration distributions between the numerical results obtained using the present model and analytical solutions based on Eq. (26) at 1.25 s. Figure 4 compares the concentration contour at 1.25 s; the data show that the numerical results agree well with the analytical solutions.

3 Laboratory experiments

3.1 *Experimental setup*

The results presented in this paper are based on measure-

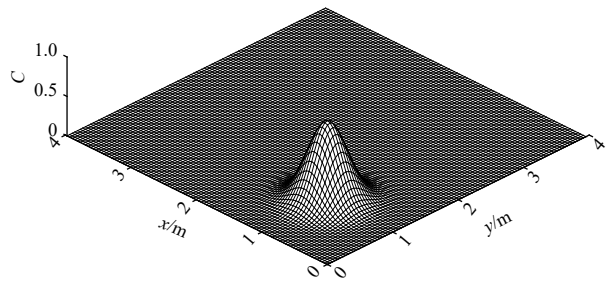

Fig. 2. The initial Gaussian pulse.

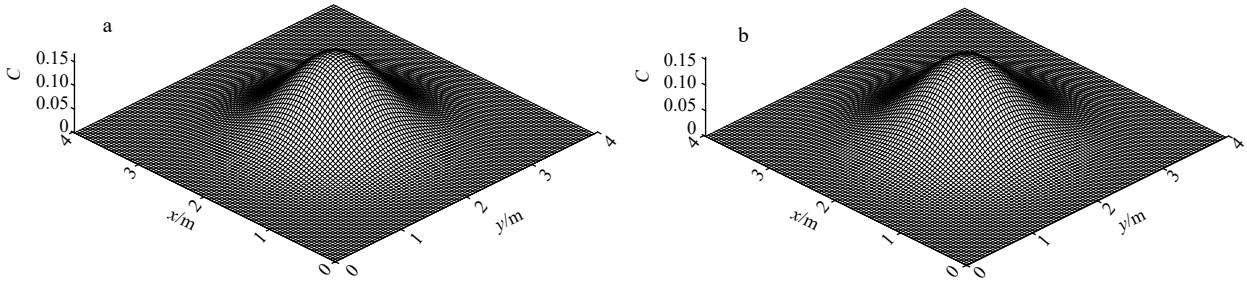

Fig. 3. Concentration distributions by analytical and numerical solutions after 1.25 s. a. Analytical solution; b. numerical solution.

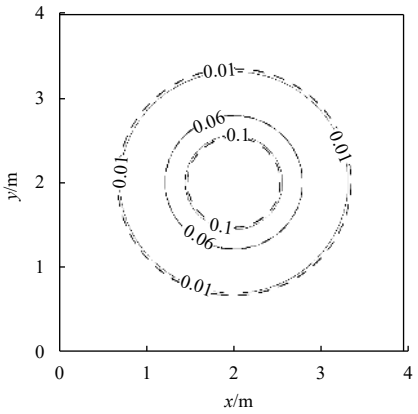

Fig. 4. Concentration contour for advection and diffusion by analytical (solid line) and numerical (dash line) solutions after 1.25 s.

ments collected within the wave basin at the State Key Laboratory of Coastal and Offshore Engineering, Dalian University of Technology. This facility is 55 m in length, 34 m in width, and 1.0 m in depth; the experimental layout and bottom profile are shown in Fig. 5. In this case, the beach forms an angle of 30° with respect to the wave generator to create a large angle of incidence; this equates to a longer beach and thus more room for alongshore currents to develop. A plane concrete profile with a slope of 1:100 was constructed, and the still-water depth over the horizontal bottom was 0.18 m. A wave generator consisting of individual wave paddles is located at the offshore end of the basin and has a total length of 24.5 m. The paddles were moved in phase with one another in all experiments.

A dye-release experiment was conducted to observe spatial patch motions visually, and an alongshore current was induced. The dye (substituted with ink in this case) was therefore released continuously into the surf zone through a long thin tube (0.8 cm in diameter). The dye-release locations were at approximately

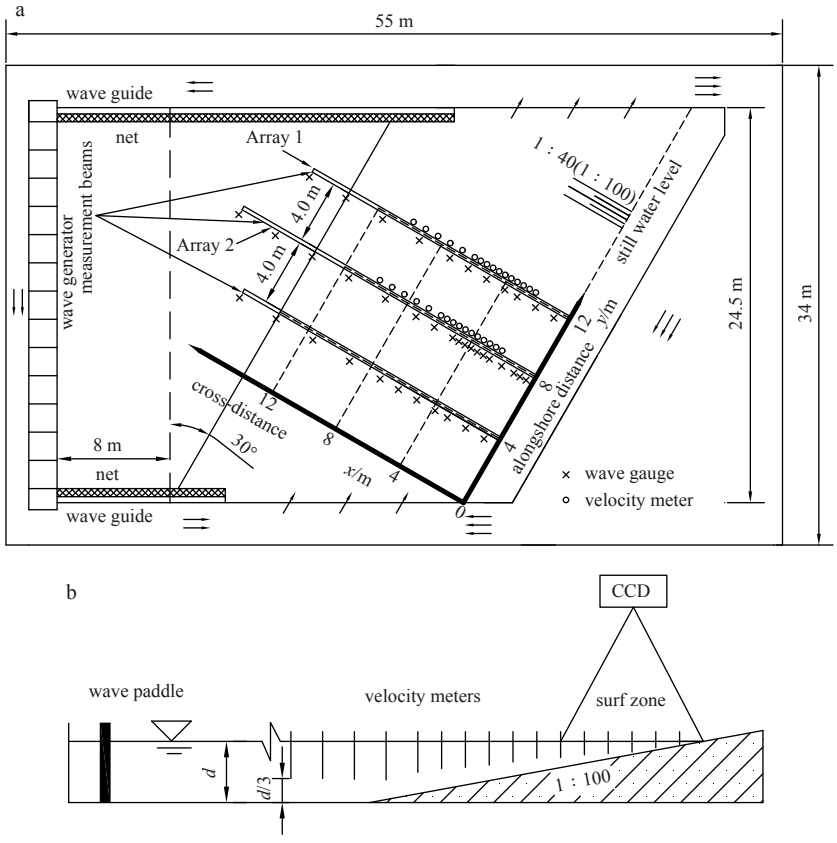

Fig. 5. Experimental layout (a) and bottom profile (b).

$x = 4.5$ m and $y = 3$ m for the 1:100 slope, and the depth of release was at approximate one third of water depth from the bottom. The dye-patch image was recorded using a charge-coupled device (CCD) launched at a height of about 8 m above the water surface (Fig. 5b). The plane beach in this experiment was painted white, and square grids (1 m × 1 m) were drawn on the surface to facilitate more precise analysis of the dye transport. Patch shape and the trajectory of maximum concentration were therefore visualized, but contours at different times cannot be given because the concentrations were not recorded. Nevertheless, dye-patch pictures taken using CCD are sufficient for this numerical analysis because our emphasis is on the role played by Stokes drift in dye transport within the surf zone as well as on how the trend, or trajectory, of this movement is influenced by this process. It is well-known that pollutant transport trends and trajectories are very important for the design of outfalls in coastal regions.

To make alongshore currents recirculate within the wave basin and produce uniform movements, a circulation channel was introduced around the beach with a width of 3.0 m at the two lateral ends and a depth of 1.0 m (the same as in the horizontal bottom part of the basin). Free surface elevations were measured in this experiment using 40 capacity wave gauges deployed in three arrays normal to the shoreline, and 32 two-dimensional velocity meters (VMs) were distributed in two identical arrays of 16 in each case (Fig. 5). These VMs were used to measure the flow field at a sampling rate of 20 Hz and were set at one-third water depth from the bottom (Fig. 5), which was approximately the location of the depth-averaged alongshore currents. The distance of VMs from the shoreline, x, is given in Table 1. All the velocity meters used in this analysis were strain type because this form works well over long horizontal time period oscillations (longer than 2 s). This experimental setup is acceptable for the measurement of long-period unstable alongshore current motions, as described in this analysis.

A series of monochromatic and unidirectional obliquely incident waves were then generated. Table 2 outlines the conditions used in these experiments.

The procedure followed for each experiment involved the initial creation of a uniform alongshore current. Current velocities were then measured for 4 min as regular waves passed along the basin, and the deformation of the dye patch was observed using the CCD system as mean alongshore currents settled.

Table 1. The distances of velocity meters from the shoreline

VM	x/m slope (1:100)	VM	x/m slope (1:100)
1	2.0	9	6.0
2	2.5	10	6.5
3	3.0	11	7.0
4	3.5	12	8.0
5	4.0	13	9.0
6	4.5	14	10.0
7	5.0	15	11.0
8	5.5	16	12.0

Table 2. Test conditions

Case	Incident wave	Slope	Still water depth/cm	Mean wave height H/cm	Peak period T/s
1	regular	1:100	18	4.5	1.0
2	regular	1:100	18	2.7	1.5

3.2 *Experimental results*

The data presented in Fig. 6 reveal that predicted mean alongshore current, wave height, and mean free surface in both Cases 1 and 2 agree well with measurements. We can therefore validate our present numerical model on the basis of both tests and experiments.

Figure 7 shows the deformation of the dye patch at $t = 40$ s, $t = 50$ s, $t = 60$ s and $t = 70$ s for Case 2 and the corresponding contours in the physical coordinate system obtained through coordinate transformation (Holland et al., 1997).

As discussed, a long thin tube was used to release dye continuously into the water at a discharge rate of about 50 cm^3/s. Hence, because the still-water depth h was 18 cm, the source term $S_m = Q/h = 2.77 \times 10^{-4}$ m^2/s can be used to simulate pollutant transport.

The concentration contours for the two cases were then modeled using our existing system, and the following normalization was introduced:

$$C' = \frac{C}{C_{max}}, \tag{28}$$

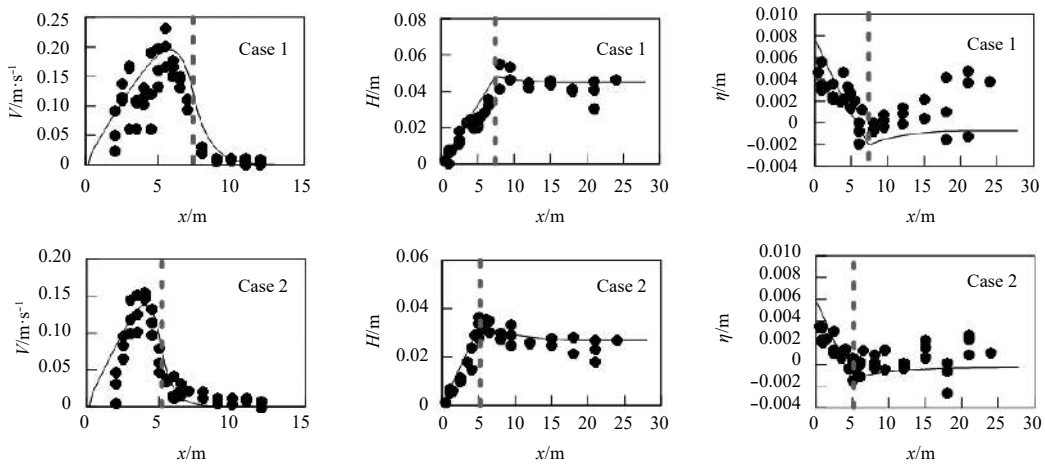

Fig. 6. Cross-shore profiles of mean longshore currents, wave height and set-up of mean water level for Case 1 ($T = 1$ s, $H = 3.5$ cm, $\theta = 30°$, slope: 1:100) and Case 2 ($T = 1.5$ s, $H = 2.7$ cm, $\theta = 30°$, slope: 1:100). Black dot: experimental data; solid line: numerical results. In all plots, dashed gray line indicates the breaker line.

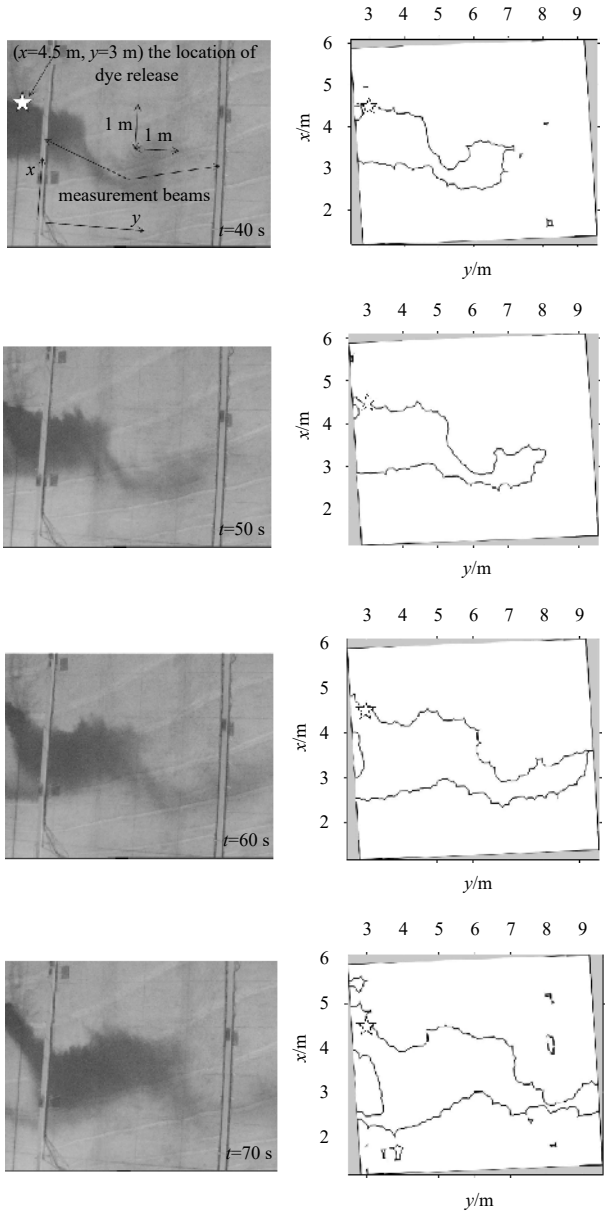

Fig. 7. Deformation of the dye patch at t=40 s, 50 s, 60 s and 70 s for Case 2 (left array) and contour transformed from pixel coordinate into the physical coordinate (right array) (star indicates the location of release).

where C_{max} denotes the maximum concentration across the entire computational domain, which enables the dimensionless concentration contour to be obtained. A value of C'=5% is given only to compare with dye-patch shape; hence, the concentration at the boundary of the dye patch is regarded as approximately 5% of the maximum.

3.3 *Final dye-patch inclination angle to reach the shoreline*

We examined the final inclination angle required for the continuously released pollutant plume to reach the shoreline under the two cases. The final angle between the line connecting the source and centroid of the dye patch and the shoreline was referred to as the final inclination angle and denoted by θ_t, as shown in Fig. 8.

Pollution transport in a pure wave field depends entirely on

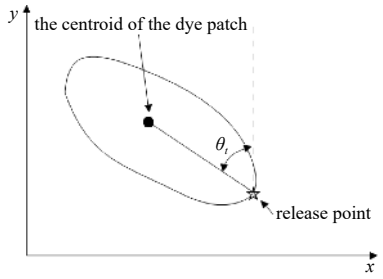

Fig. 8. Schematics defining the inclination angle.

incoming wave properties. This means that pollution will move inside the surf zone in a direction perpendicular to the wave crest line under monochromatic and unidirectional obliquely incident waves. Pollution transport in the surf zone becomes much more complex, however, because of wave breaking and shallow water. Coastal engineers must therefore pay much more attention to trends in dye-patch transport within this zone when they design marine outfalls or consider safety issues during spills. We have examined dye transportation direction within the surf zone on a plane beach in this study considering two cases. It is clear that the centroid of a dye patch is an important parameter when describing its movement trajectory; the center of such a distribution, $(x_c(t), y_c(t))$, was calculated as follows:

$$x_c(t) = \frac{1}{N}\sum x \cdot g(x,y,t), \tag{29}$$

$$y_c(t) = \frac{1}{N}\sum y \cdot g(x,y,t), \tag{30}$$

where N denotes the number of pixels with $g(x, y, t)$=1 in the image. Hence, the inclination angle, θ_t, was calculated using the slope of the line connecting the release point and the centroid of the dye patch. Figure 9 shows the centroids of dye patches at different times for the two cases considered here. These results show that the dye patch remained very close to the shoreline after 70 s in both cases, the inclination angles, θ_t, for case 1 and case 2 at 70 s were 24.7° and 23.1°, respectively, and both wave incident angles were 30°. This means that the final inclination angles required for the dye patch to reach the shoreline are close to wave incident angles under present conditions. It will therefore be valuable in the case of coarse pollution transportation forecasting adjacent to the surf zone if we can develop this relationship between inclination and wave incident angles in future research. We show that pollutants released into the surf zone will eventually reach the shoreline and remain at this point.

4 Comparison of experimental and numerical results

Experimental (thick solid line) and numerical results with (thick dashed line) or without (thin solid line) Stokes drift for the period between 10 s and 70 s in Case 1 are shown in Fig. 10, and the same results for Case 2 are shown in Fig. 11. Experimental results suggest that the dye patch slowly moves shoreward over time and is transported rapidly in alongshore direction. Figure 12 shows the relationships between the distance (L) of the dye patch from the shoreline in a shoreward direction and time in both Case 1 and Case 2. We also performed linear fitting with our experimental data for the period between 10 s and 40 s in both cases (Fig. 12). These data show that the dye patch moved shoreward at an approximate speed of 0.05 m/s (0.017 m/s) between

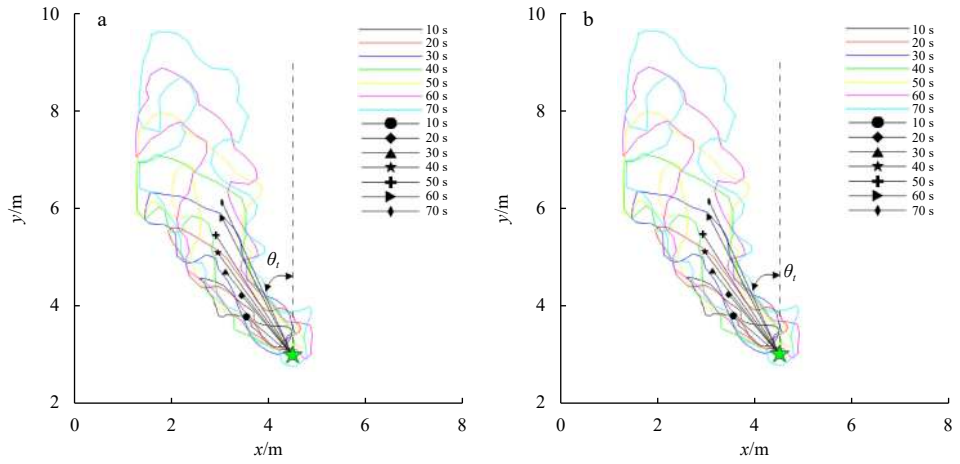

Fig. 9. Displacement of the centroid of dye patch with time for Cases 1 (a) and 2 (b). The solid lines indicate the time evolution of the isocontour C'=5%; the black symbols denote the centroid of dye patch at different time; the green star depicts the location of release; and the dashed line parallels to the shoreline.

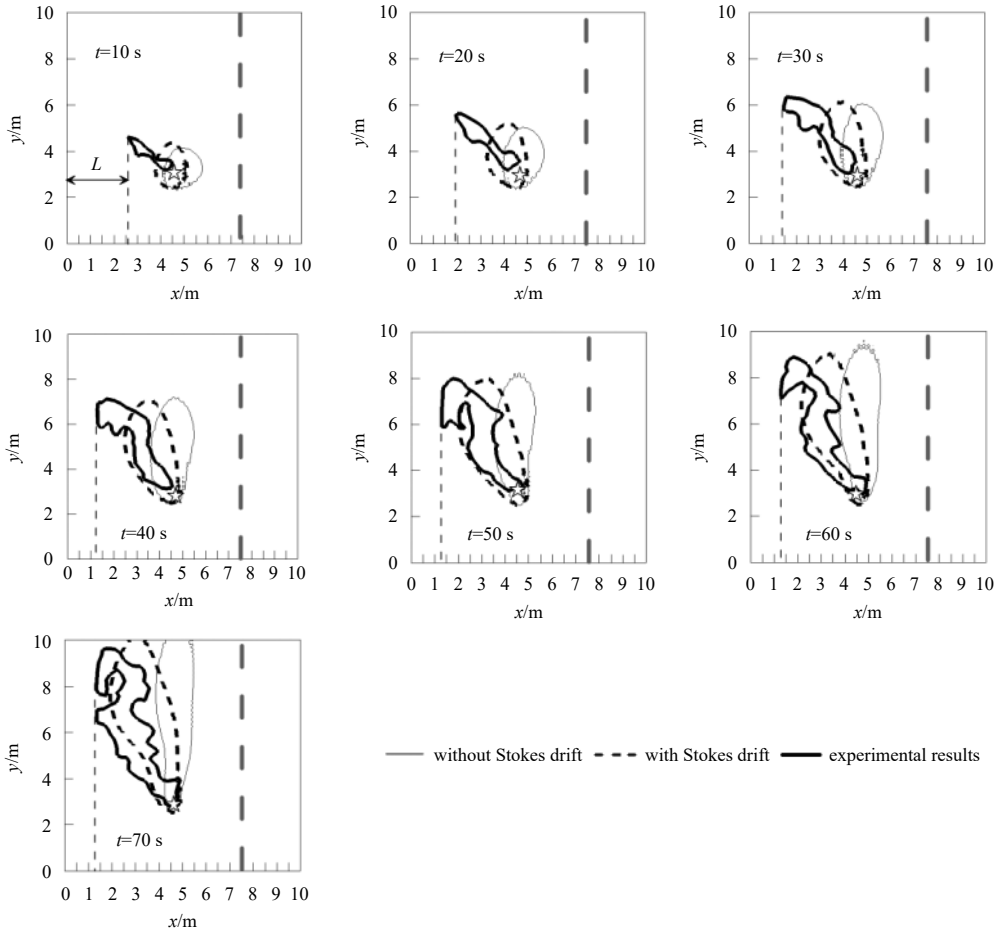

Fig. 10. The comparisons between the experimental (dark line) and numerical results with (dashed line) and without (light line) Stokes drift from 10 s to 70 s for Case 1. Dashed gray dashed line indicates the breaker line and star depicts the location of release; and thin dashed line indicates the distance (L) of the dye patch from the shoreline.

10 s and 40 s and at 0.001 m/s (0.011 m/s) after 40 s in Case 1 (2). In earlier work, Tamura et al. (2012) noted that the annual mean surface Stokes drift field ranges between 0.02 m/s and 0.10 m/s in the North Pacific; our result agrees with this earlier calculation. Indeed, the results of this study suggest that Stokes drift does have an effect on dye transport in the nearshore zone even though breaking does also take place. This corroborates the earlier result of McWilliams and Restrepo (1999), who argued that Stokes drift does influence general ocean circulation through rearrangement of surface layer dynamics. As discussed, this analys-

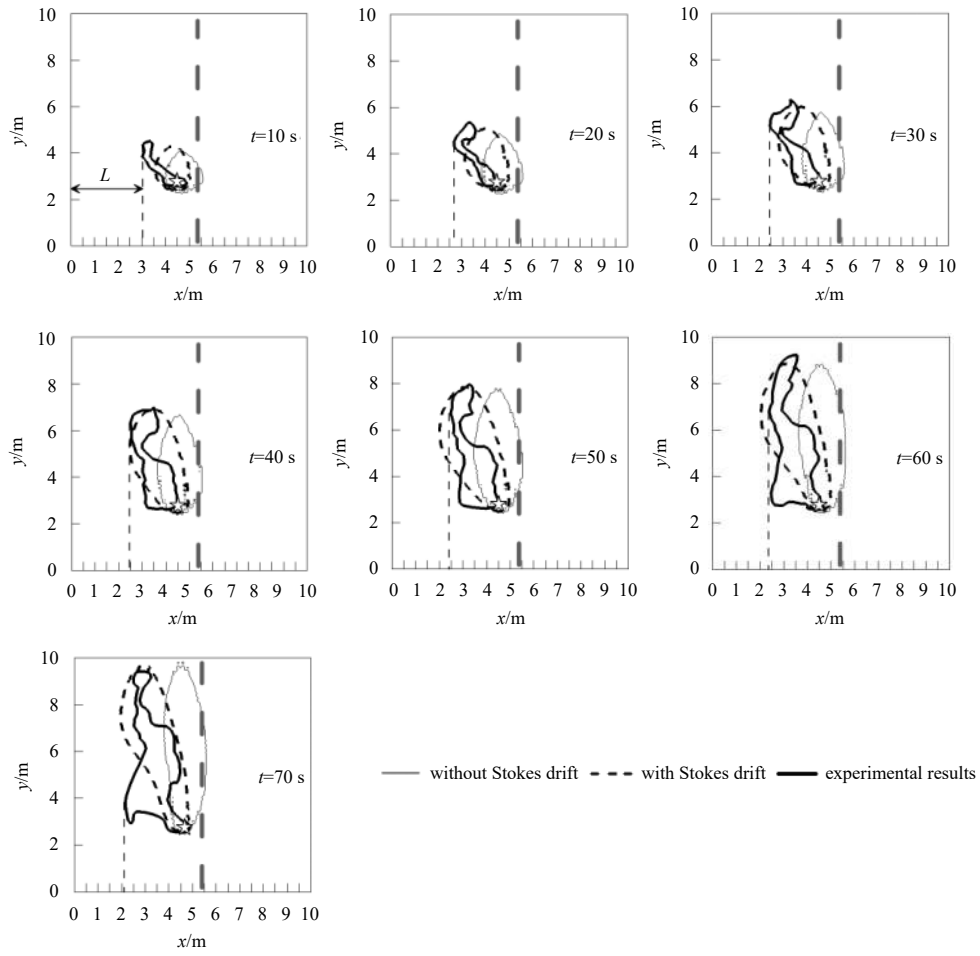

Fig. 11. The comparisons between the experimental (dark line) and numerical results with (dashed line) and without (light line) Stokes drift from 10 s to 70 s for Case 2. Dashed gray dashed line indicates the breaker line and star depicts the location of release; and thin dashed line indicates the distance (L) of the dye patch from the shoreline.

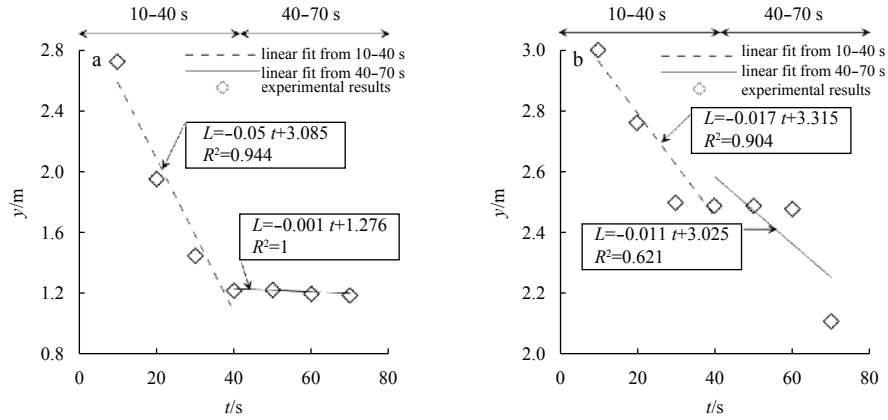

Fig. 12. The relationship between L (the distance of dye patch and the shoreline in shoreward direction) and time for Cases 1 (a) and 2 (b).

is was motivated by a desire to understand the effects of this process on transport within the nearshore zone.

Comparisons of our numerical results with and without Stokes drift versus the experimental results presented in Figs 10 and 11 reveal that trends in both agree well with one another in both test cases. It is obvious that Stokes drift exerts a considerable influence on dye transport within the surf zone. Calculated velocity components for this effect are reported in Fig. 13; these show that the Stokes drift component α_s exerts much more influence on pollutant transport in the cross-shore direction compared to alongshore (Fig. 13). Indeed, a dye patch will eventually travel close to the shoreline when spreading laterally by diffu-

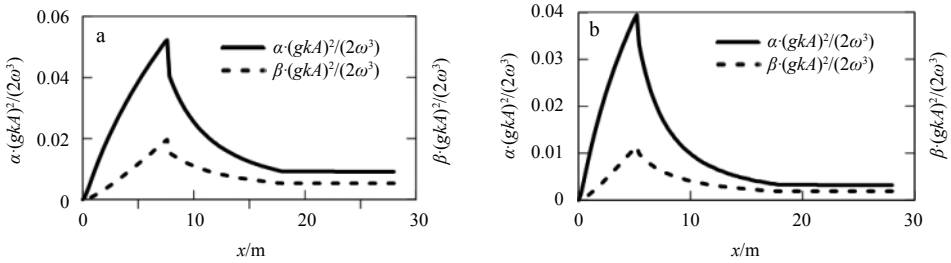

Fig. 13. Predicted cross-shore (solid line) and longshore (dashed line) Stokes drift velocity. a. Case 1 and b. Case 2.

sion, a pattern that we have also observed in the laboratory.

5 Conclusions

This study has investigated the effects of Stokes drift on the shoreward transport of a dye patch. Experimental results suggest that the dye patch moved shoreward with an approximate speed of 0.05 m/s (0.017 m/s) between 10 s and 40 s and then at 0.001 m/s (0.011 m/s) after 40 s in Case 1 (2). We also present a numerical model for pollutant transport in the surf zone; in this case, Stokes drift is included within the advective diffusion equation that expresses the transport and spreading of a solute within this zone. We then corroborate the use of our model to simulate pollutant transport within the surf zone on a plane beach using experiments. Results show that numerical data that include Stokes drift agree better with our experimental results than those that do not include this process. We show that, in general, a pollutant will be obviously transported shoreward in addition to any expected transport along the shore. We therefore suggest that Stokes drift plays an important role in pollutant drift in the surf zone, especially shoreward. Our results mean that pollutants released continuously into the surf zone will eventually reach the shoreline and be retained at this position. As noted previously by Winckler et al. (2013), the key parameter that controls this relationship is contact distance, which should be carefully taken into account in the design of marine outfalls and in the assessment of safety issues during spills. The numerical model presented in this study can be used for approximate quantification of contact distance, although dye-patch irregularities in the horizontal dimension caused by shear instabilities cannot be accurately simulated in this approach. Much research remains to be done if we are to improve the model expounded in this paper. Further detailed analyses should be carried out to investigate the effects of source position, local wave conditions, and bathymetry on dye-patch transport.

References

Apotsos A, Raubenheimer B, Elgar S, et al. 2008. Testing and calibrating parametric wave transformation models on natural beaches. Coastal Engineering, 55(3): 224–235, doi: 10.1016/j.coastaleng.2007.10.002

Baldock T E, Holmes P, Bunker S, et al. 1998. Cross-shore hydrodynamics within an unsaturated surf zone. Coastal Engineering, 34(3-4): 173–196, doi: 10.1016/S0378-3839(98)00017-9

Battjes J A, Janssen J P F M. 1978. Energy loss and set-up due to breaking of random waves. In: Proceedings of 16th Conference on Coastal Engineering. Hamburg, Germany: ASCE, 569–587

Brown J, MacMahan J, Reniers A, et al. 2009. Surf zone diffusivity on a rip-channeled beach. Journal of Geophysical Research, 114(C11): C11015, doi: 10.1029/2008JC005158

Clark D B, Feddersen F, Guza R T. 2010. Cross-shore surfzone tracer dispersion in an alongshore current. Journal of Geophysical Research, 115(C10): C10035, doi: 10.1029/2009JC005683

Clark D B, Feddersen F, Guza R T. 2011. Modeling surf zone tracer plumes: 2. Transport and dispersion. Journal of Geophysical Research, 116(C11): C11028, doi: 10.1029/2011JC007211

Clarke L B, Ackerman D, Largier J. 2007. Dye dispersion in the surf zone: measurements and simple models. Continental Shelf Research, 27(5): 650–669, doi: 10.1016/j.csr.2006.10.010

Curcic M, Chen S S, Özgökmen T M. 2016. Hurricane-induced ocean waves and stokes drift and their impacts on surface transport and dispersion in the Gulf of Mexico. Geophysical Research Letters, 43(6): 2773–2781, doi: 10.1002/grl.v43.6

Ebersole B A, Dalrymple R A. 1980. Numerical modelling of nearshore circulation. In: Proceedings of the 17th International Conference on Coastal Engineering. Sydney, Australia: ASCE, 2710–2725

Grant S B, Kim J H, Jones B H, et al. 2005. Surf zone entrainment, along-shore transport, and human health implications of pollution from tidal outlets. Journal of Geophysical Research, 110(C10): C10025, doi: 10.1029/2004JC002401

Hally-Rosendahl K, Feddersen F, Guza R T. 2014. Cross-shore tracer exchange between the surfzone and inner-shelf. Journal of Geophysical Research, 119(7): 4367–4388

Harris T F W, Jordaan J M, McMurray W R, et al. 1963. Mixing in the surf zone. Air and Water Pollution, 7: 649–667

Holland K T, Holman R A, Lippmann T C, et al. 1997. Practical use of video imagery in nearshore oceanographic field studies. IEEE Journal of Oceanic Engineering, 22(1): 81–92, doi: 10.1109/JOE.48

Inman D L, Tait R J, Nordstrom C E. 1971. Mixing in the surf zone. Journal of Geophysical Research, 76(15): 3493–3514, doi: 10.1029/JC076i015p03493

Iwasaki S, Isobe A, Kako S, et al. 2017. Fate of microplastics and mesoplastics carried by surface currents and wind waves: a numerical model approach in the Sea of Japan. Marine Pollution Bulletin, 121(1–2): 85–96, doi: 10.1016/j.marpolbul.2017.05.057

Jacobsen N G. 2016. Wave-averaged properties in a submerged canopy: energy density, energy flux, radiation stresses and Stokes drift. Coastal Engineering, 117: 57–69, doi: 10.1016/j.coastaleng.2016.07.009

Lentz S J. 2008. Observations and a model of the mean circulation over the Middle Atlantic Bight continental shelf. Journal of Physical Oceanography, 38(6): 1203–1221, doi: 10.1175/2007JPO3768.1

Longuet-Higgins M S. 1970a. Longshore currents generated by obliquely incident sea waves: 1. Journal of Geophysical Research, 75(33): 6778–6789, doi: 10.1029/JC075i033p06778

Longuet-Higgins M S. 1970b. Longshore currents generated by obliquely incident sea waves: 2. Journal of Geophysical Research, 75(33): 6790–6801, doi: 10.1029/JC075i033p06790

McWilliams J C, Restrepo J M. 1999. The wave-driven ocean circulation. Journal of Physical Oceanography, 29(10): 2523–2540, doi: 10.1175/1520-0485(1999)029<2523:TWDOC>2.0.CO;2

Myrhaug D, Wang Hong, Holmedal L E. 2018. Stokes transport in layers in the water column based on long-term wind statistics. Oceanologia, 60(3): 305–311, doi: 10.1016/j.oceano.2017.12.004

Özkan-Haller H T, Kirby J T. 1999. Nonlinear evolution of shear instabilities of the longshore current: a comparison of observations and computations. Journal of Geophysical Research, 104(C11): 25953–25984, doi: 10.1029/1999JC900104

Pearson J M, Guymer I, West J R, et al. 2009. Solute mixing in the surf zone. Journal of Waterway, Port, Coastal, and Ocean Engineering, 135(4): 127–134, doi: 10.1061/(ASCE)0733-950X(2009)135:4(127)

Roelvink J A. 1993. Surf beat and its effect on cross-shore profiles [dissertation]. TU Delft: Delft University of Technology

Sun Tao, Tao Jianhua. 2006. Numerical simulation of pollutant transport acted by wave for a shallow water sea bay. International Journal for Numerical Methods in Fluids, 51(5): 469–487, doi: 10.1002/(ISSN)1097-0363

Svendsen I A, Putrevu U. 1994. Nearshore mixing and dispersion. Proceedings of the Royal Society A: Mathematical, Physical and Engineering Sciences, 445(1925): 561–576, doi: 10.1098/rspa.1994.0078

Tamura H, Miyazawa Y, Oey L Y. 2012. The Stokes drift and wave induced-mass flux in the North Pacific. Journal of Geophysical Research, 117(C8): C08021, doi: 10.1029/2012JC008113

Tang Jun, Lyu Y, Shen Yongming. 2016. Numerical simulation of sediment transport in coastal waves and wave-induced currents. Acta Oceanologica Sinica, 35(9): 111–116, doi: 10.1007/s13131-016-0932-8

Tang Jun, Lyu Y, Shen Yongming, et al. 2017. Numerical study on influences of breakwater layout on coastal waves, wave-induced currents, sediment transport and beach morphological evolution. Ocean Engineering, 141: 375–387, doi: 10.1016/j.oceaneng.2017.06.042

van Rijn L C. 1986. Sedimentation of dredged channels by currents and waves. Journal of Waterway, Port, Coastal, and Ocean Engineering, 112(5): 541–559, doi: 10.1061/(ASCE)0733-950X(1986)112:5(541)

Weisberg R H, Zheng Lianyuan, Liu Yonggang. 2017. On the movement of Deepwater Horizon Oil to northern Gulf beaches. Ocean Modelling, 111: 81–97, doi: 10.1016/j.ocemod.2017.02.002

Winckler P, Liu P L F, Mei C C. 2013. Advective diffusion of contaminants in the surf zone. Journal of Waterway, Port, Coastal, and Ocean Engineering, 139(6): 437–454, doi: 10.1061/(ASCE)WW.1943-5460.0000196

Xu Ming, Chua V P. 2016. A numerical study on flow and pollutant transport in Singapore coastal waters. Marine Pollution Bulletin, 111(1–2): 160–177, doi: 10.1016/j.marpolbul.2016.07.014

Zhao Qun, Svendsen I A, Haas K. 2003. Three-dimensional effects in shear waves. Journal of Geophysical Research, 108(C8): 3270, doi: 10.1029/2002JC001306